Electronic Supplementary Information for

Porous structure, carbon dioxide capture and separation in crosslinked porphyrin-based polyimides networks

Kaixiang Shi [a], Hongyan Yao [a], Shuai Zhang [a], Yanfeng Wei [c], Wenhan Xu [a], Ningning Song [a], Shiyang Zhu [a], Ye Tian [a], Yongcun Zou [b,*] and Shaowei Guan [a,*]

[a] Key Laboratory of High Performance Plastics (Jilin University), Ministry of Education, National & Local Joint Engineering Laboratory for Synthesis Technology of High Performance Polymer, Jilin University, Qianjin Street 2699, Changchun, 130012, People's Republic of China.

[b] State Key Laboratory of Inorganic Synthesis and Preparative Chemistry, College of Chemistry, Jilin University, Changchun 130012, China.

[c] DWI - Leibniz-Institut für Interaktive Materialien e.V, Forckenbeckstraße 50, D-52056 Aachen.

[*] Corresponding authors. E-mail address: zouyc@jlu.edu.cn (Y. Zou), guansw@jlu.edu.cn (S. Guan).

Contents

Figure S3. TGA curves of samples under nitrogen atmosphere.

Figure S4. TGA curves of PPBPI-CRs under air atmosphere.

Figure S5. Powder XRD spectra of samples.

Figure S6. FE-SEM images of samples.

Figure S7. EDS mapping photographs of PPBPI-Mn-CR.

Figure S8. EDS mapping photographs of PPBPI-Fe-CR.

Figure S9. HR-TEM image of PPBPI-H-CR.

Figure S10. HR-TEM image of PPBPI-Mn-CR.

Figure S11. HR-TEM image of PPBPI-Fe-CR.

Figure S12. Adsorption (filled) and desorption (empty) isotherms of N_2 at 77 K for PPBPIs.

Figure S13. Adsorption selectivity of CO_2 over N_2 and CH_4 for PPBPI-CRs.

Figure S14. (a) Adsorption (filled) and desorption (empty) isotherms of N_2 at 77 K for Fe-PPBPI-CR, (b) pore size distribution of Fe-PPBPI-CR based on NLDFT method.

Figure S15. CO_2 and N_2 adsorption and desorption isotherms for Fe-PPBPI-CR at 273 and 298 K, adsorption selectivity of CO_2 over N_2 for Fe-PPBPI-CR.

Figure S16. EDS mapping photographs of Fe-PPBPI -CR.

Scheme S1. Synthesis routes to crosslinked metalloporphyrin-based polyimide networks (Fe-PPBPI-CR) from metalloporphyrin-based monomer.

Supplementary method.

Materials: Diphenyl sulfone, 1-methyl-2-pyrrolidinone (NMP) and isoquinoline were purchased from Aladdin Industrial. Inc. Ethanol and acetone were provided by Beijing chemical works. Ferrous chloride tetrahydrate, and manganese acetate tetrahydrate were obtained from Energy chemical (China). All chemical reagents were used as received unless otherwise stated.

Instruments and general methods

Fourier transform infrared (FT-IR) spectra were carried out on a Nicolet Impact 410 Fourier-transform infrared spectrometer ranging from 400 to 4000 cm^{-1} by means of mixing the samples with KBr. Solid-state ^{13}C cross-polarization magic angle spinning (CP/MAS) NMR spectra of solid samples were performed on a Bruker AVANCE Ⅲ 400 WB solid 400 megabyte (wide cavity) superconducting NMR spectrometer. Elemental microanalyses were performed at the Vario EL cube to comfirm the contents of carbon, hydrogen, and nitrogen of the produced samples. Powder X-ray diffractions (PXRD) using Cu Kα radiation from 5° to 40° were performed on the PANalytical B.V. Empyrean to confirm the morphologies of synthesized samples. Thermogravimetry analyses (TGA) were measured on a Perkin-Elmer TGA-7 thermo-gravimetric analyzer at a heating rate of 10 ℃/min from 100 to 800 ℃ in nitrogen/air atmosphere. Differential scanning calorimetry (DSC) was carried out on a TA Q2000 at a heating rate of 10 ℃ min^{-1} from 100 to 450 ℃ under a nitrogen atmosphere to characterize polymer exothermic peaks. Field-emission scanning electron microscopy (FE-SEM) experiments were recorded on a SU8020 model HITACHI microscope, and the powder samples were sputtered with platinum prior to measure. Transmission electron microscopy (TEM) was collected on a JEOL model JEM-2100 micro-scope to view the pore channels of PPBPI-CRs. Nitrogen adsorption and desorption of polymers were recorded on a micromeritics ASAP 2020 analyzer at 77 K with polymers degassed at 200 ^oC to remove the gas and the residual solvents trapped in pore channels prior to measure. The specific surface areas were calculated from Brunauer-Emmett-Teller (BET) model in the relative pressure region of $P/P_0 = 0.05 - 0.3$. The total pore volume was calculated at $P/P_0 = 0.99$, and micropore volume was collected using t-Plot method. CO_2 sorption isotherms were recorded on a Micro Meritics Tristar Ⅱ 3020 surface area, the CO_2 uptakes of PPBPI-CRs were calculated from CO_2 sorption isotherms. CO_2 isosteric enthalpies of adsorption were calculated using the virial and Clausius-Clapeyron equations at 273 and 295 K. The pore size distributions of PPBPI-CRs based on Nonlocal Density Functional Theory (NLDFT) were calculated from carbon dioxide sorption isotherms at 273 K. The sorption isotherms of N_2 and CH_4 at 273 K were measured and compared with those of CO_2 to calculate the separation properties of

PPBPI-CRs, which were calculated from initial slopes of pure-component sorption isotherms.

Synthesis of crosslinked porphyrin-based polyimides

Synthesis of porphyrin-based polyimide (PPBPI-H)

In a 250 mL three-necked flask equipped with mechanical stirrer, nitrogen inlet, drying tube and constant pressure drop funnel under nitrogen atmosphere, TAPP (0.6 g, 0.8892 mmol) dissolved in 30 mL NMP were added. Subsequently, PEPHQDA (0.6033 g, 0.8892 mmol) dissolved in 24 mL NMP were added dropwise into the flask. The mixture solution was reacted at atmospheric temperature and maintained overnight. Then 2.5 mL isoquinoline was added to facilitate the reaction. The reaction was heated to 120 ^{o}C and kept for 4 h, followed heating to 180 ^{o}C and maintained for 24 h. After cooling to room temperature, the mixture solution was poured into 500 mL ethanol to give the precipitate. The precipitate was isolated by filtration and purified in a Soxhlet apparatus for 24 h with ethanol and dried at 100 ^{o}C under vacuum to afford PPBPI-H. Yield: 80%.

Synthesis of metalloporphyrin-based polyimides (PPBPI-Mn and PPBPI- Fe)

In a 250 mL three-necked flask with mechanical stirrer, drying tube and nitrogen inlet under nitrogen atmosphere, PPBPI-H (0.28 g), $Mn(CH_3COO)_2{\cdot}4H_2O$ (0.725 g, 2.96 mmol) and 80 mL DMF were added. The mixture was heated to 100 ^{o}C and maintained for 8 h. After cooling to room temperature, the reaction solution was poured into 800 mL deionized water to give the precipitate. The resultant product was isolated by filtration and washed thoroughly using deionized water. Yield: 92%.

PPBPI-Fe was synthesized as the same synthetic route as PPBPI-Mn except that $FeCl_2{\cdot}4H_2O$ was replaced by $Mn(CH_3COO)_2{\cdot}4H_2O$. Yield: 90%.

Synthesis of PPBPI-H-CR

In a 50 mL three-necked flask equipped with mechanical stirrer, nitrogen inlet and

condenser under nitrogen atmosphere, PPBPI-H (0.2 g) and diphenyl sulfone (25 g) were added. The mixture was heated to 360 ^{o}C and maintained for 24 h to ensure that the polymers underwent post-crosslinking reaction completely. After cooling to 150 ^{o}C, the solution was poured into 300 mL acetone to give the post-crosslinked polymer. The resultant product was isolated by filtration, extracted in a Soxhlet apparatus using acetone and dried at 120 ^{o}C under vacuum to afford PPBPI-H-CR. Yield: 90%.

PPBPI-Mn-CR and PPBPI-Fe-CR were synthesized according to the same synthetic route except using PPBPI-Mn and PPBPI-Fe to replace PPBPI-H.

Synthesis of crosslinked metalloporphyrin-based polyimide from metalloporphyrin-based monomer (Fe-PPBPI-CR)

Synthesis of metalloporphyrin-based monomer (Fe-TAPP)

In a 250 mL three-necked flask equipped with mechanical stirrer, nitrogen inlet and condenser under nitrogen atmosphere, TAPP (0.3 g, 0.4446 mmol) dissolved in 30 mL DMF was added. Subsequently, ferrous chloride tetrahydrate (0.442 g, 2.223 mmol) was added into the flask. The mixture solution was reacted at 100 ^{o}C for 6 h. After cooling to room temperature, the mixture solution was poured into 500 mL deionized water to give the precipitate. The precipitate was isolated by filtration and purified in a Soxhlet apparatus for 24 h with deionized water and dried at 80 ^{o}C under vacuum to afford Fe-TAPP. Yield: 80%.

Synthesis of metalloporphyrin-based polyimide (Fe-PPBPI)

Fe-PPBPI was prepared from Fe-TAPP and PEPHQDA according to the same synthetic route of PPBPI-Fe.

Fe-PPBPI-CR was prepared from Fe-PPBPI according to the same synthetic route of PPBPI-Fe-CR.

Table S1. Elemental analysis data of samples.

Samples	Measured value		
	C	H	N
PPBPI-H-CR	74.77	3.738	6.96
PPBPI-Mn-CR	73.03	3.693	4.88
PPBPI-Fe-CR	65.94	3.235	4.69

Table S2. K_H, A_0, A_1, and Q_0 values of PPBPI-CRs from CO_2 sorption isotherms.

Samples	T	K_H	A_0	A_1	Q_0
	K	mol g^{-1} Pa^{-1}	ln(mol g^{-1} Pa^{-1})	g mol^{-1}	kJ mol^{-1}
	273	11.064×10^{-8}	-16.017	-770.993	
PPBPI-H-CR					24.5
	295	4.951×10^{-8}	-16.821	-791.265	
	273	4.603×10^{-8}	-16.894	-829.785	
PPBPI-Mn-CR					29.2
	295	1.762×10^{-8}	-17.854	-706.093	
	273	6.295×10^{-8}	-16.581	-1306.582	
PPBPI-Fe-CR					31.0
	295	2.270×10^{-8}	-17.601	-1270.716	

Table S3 Specific surface areas, pore volume, and pore size distribution in PPBPIs and PPBPI-CRs network structures.

Samples	S_{BET}[a]	$S_{Langmuir}$[b]	S_{micro}[c]	V_{total}[d]	V_{micro}[e]	V_{micro}/V_{total}	PSD[f]
	$m^2\ g^{-1}$	$m^2\ g^{-1}$	$m^2\ g^{-1}$	$cm^3\ g^{-1}$	$cm^3\ g^{-1}$		nm
PPBPI-H	167.3			0.547	0.008	0.015	
PPBPI-H-CR	733	1000	363	0.532	0.170	0.320	0.39,0.80,1.27
PPBPI-Mn	8.3			0.0349	0.002	0.057	
PPBPI-Mn-CR	144	197	92	0.124	0.044	0.355	1.18
PPBPI-Fe	10.3			0.0259	0.002	0.077	
PPBPI-Fe-CR	172	262	102	0.135	0.054	0.40	1.26

[a] The Brunauer-Emmett-Teller and [b] Langmuir surface areas of samples were collected from nitrogen sorption isotherms.

[c] The micropore surface areas were based on t-plot method.

[d] Total pore volume derived from N_2 isotherms at $P/P_0 = 0.99$.

[e] Micropore volume determined from t-plot method.

[f] Pore size distributions (PSD) were collected from nitrogen sorption isotherms based on nonlocal density functional theory.

Table S4 Specific surface areas, pore volumes, and pore size distributions in PPBPI-Fe-CR and Fe-PPBPI-CR network structures.

Samples	S_{BET}[a]	$S_{Langmuir}$[b]	V_{total}[c]	PSD[d]
	$m^2\ g^{-1}$	$m^2\ g^{-1}$	$cm^3\ g^{-1}$	nm
Fe-PPBPI-CR	526	665	0.645	0.5,1.4,2.4
PPBPI-Fe-CR	172	262	0.135	1.26

[a] The Brunauer-Emmett-Teller and [b] Langmuir surface areas of samples were collected from nitrogen sorption isotherms.

[c] Total pore volume derived from N_2 isotherms at $P/P_0 = 0.99$.

[d] Pore size distributions (PSD) were collected from nitrogen sorption isotherms based on nonlocal density functional theory.

Table S5. CO_2 uptakes from CO_2 sorption isotherms at 273 and 298 K, gas selectivity from CO_2 and N_2 sorption isotherms at 273 K.

Samples	CO_2 uptake[a] mmol g^{-1}	CO_2 uptake[b] mmol g^{-1}	Gas selectivity[c] CO_2/N_2
Fe-PPBPI-CR	1.55	0.93	41.08

[a] CO_2 uptakes derived from CO_2 sorption isotherms at 1.0 bar and 273 K.

[b] CO_2 uptakes determined at 1 bar and 298 K.

[c] The CO_2/N_2 selectivity was calculated from initial slopes of pure-component sorption isotherms.

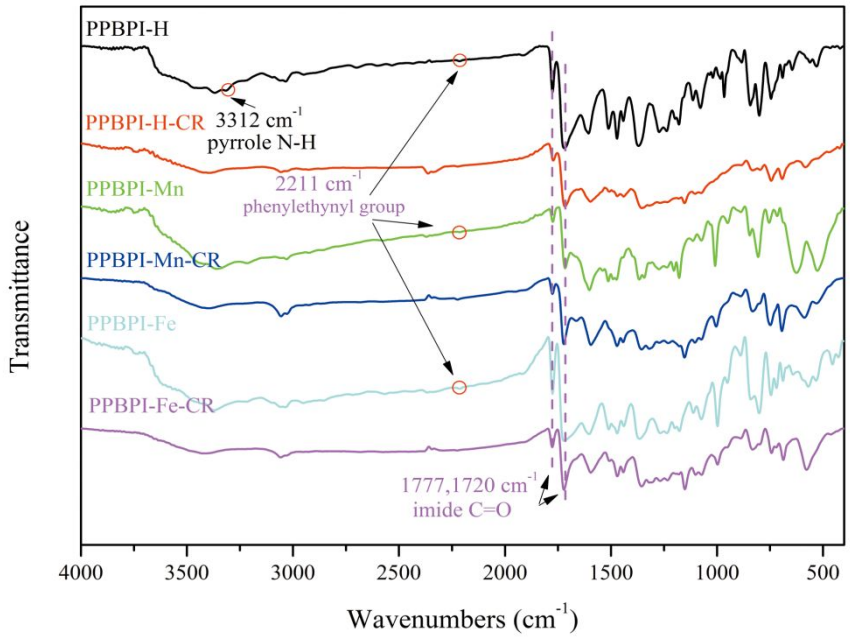

Figure S1. FTIR spectra of samples.

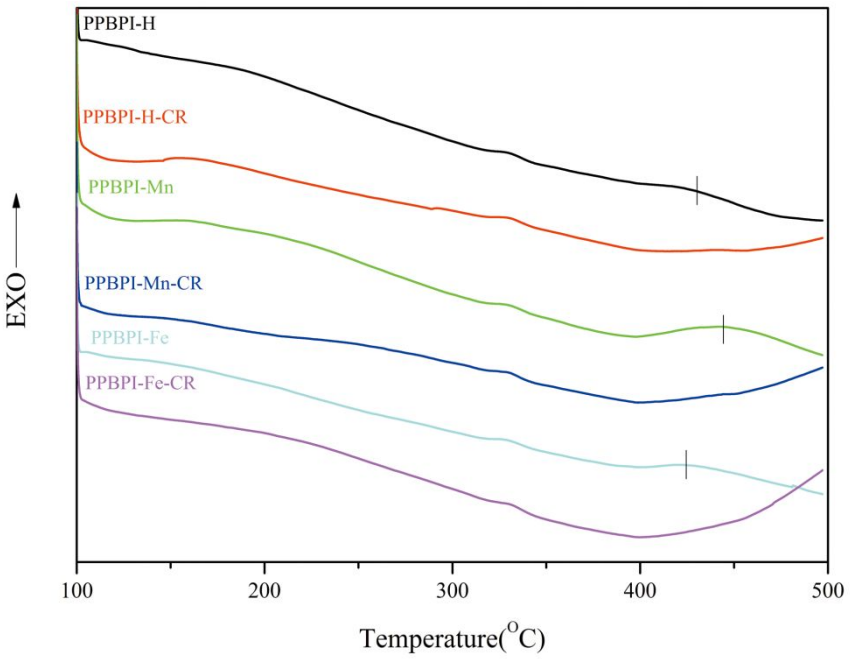

Figure S2. DSC curves of samples.

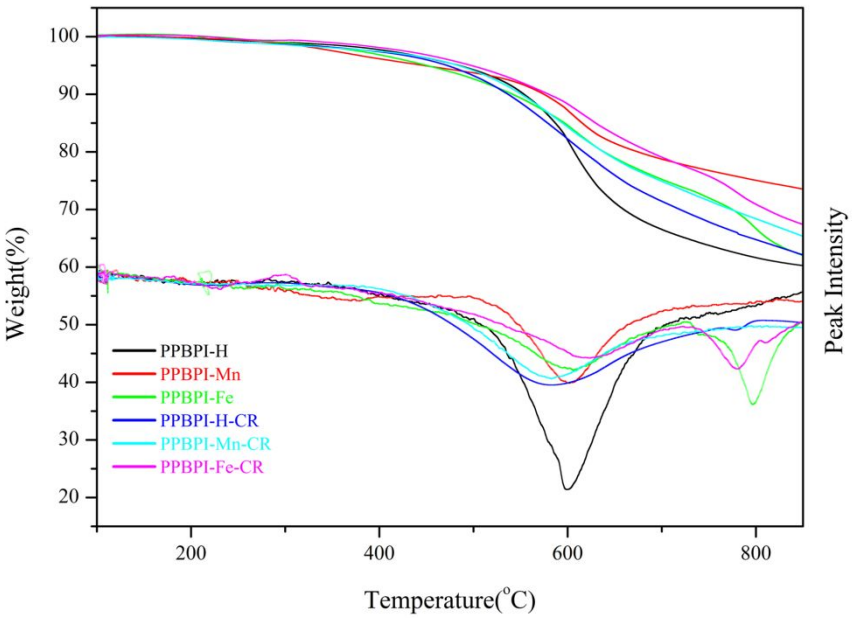

Figure S3. TGA curves of samples under nitrogen atmosphere.

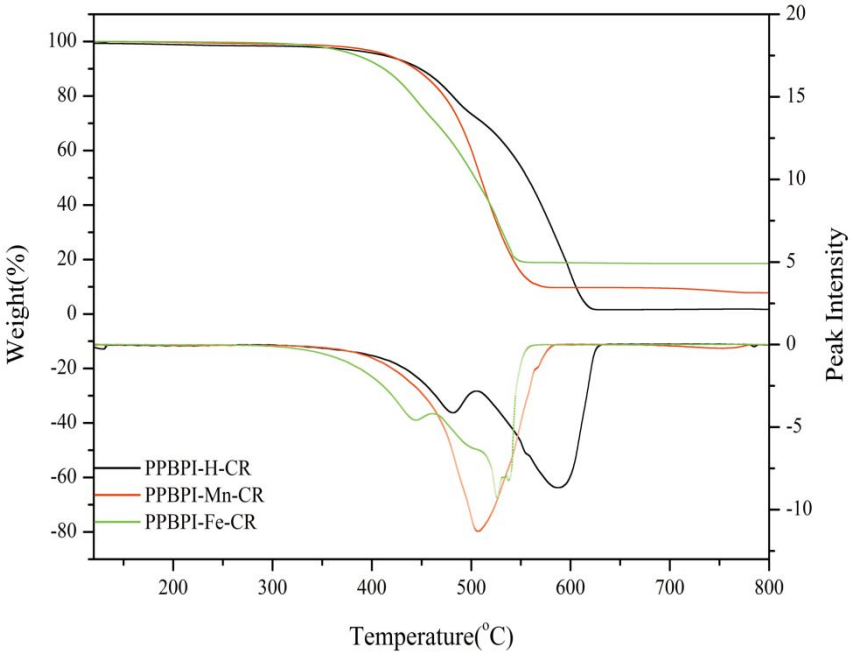

Figure S4. TGA curves of PPBPI-CRs under air atmosphere.

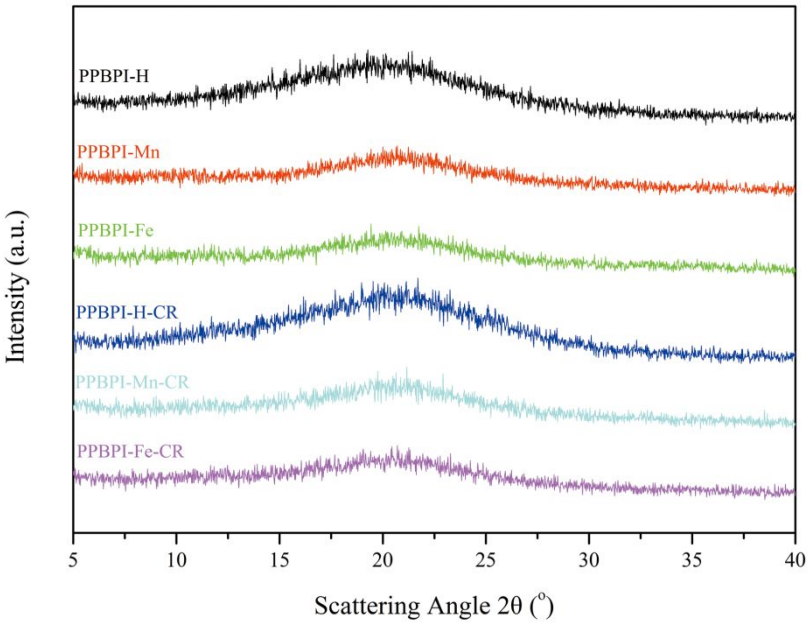

Figure S5. Powder XRD spectra of samples.

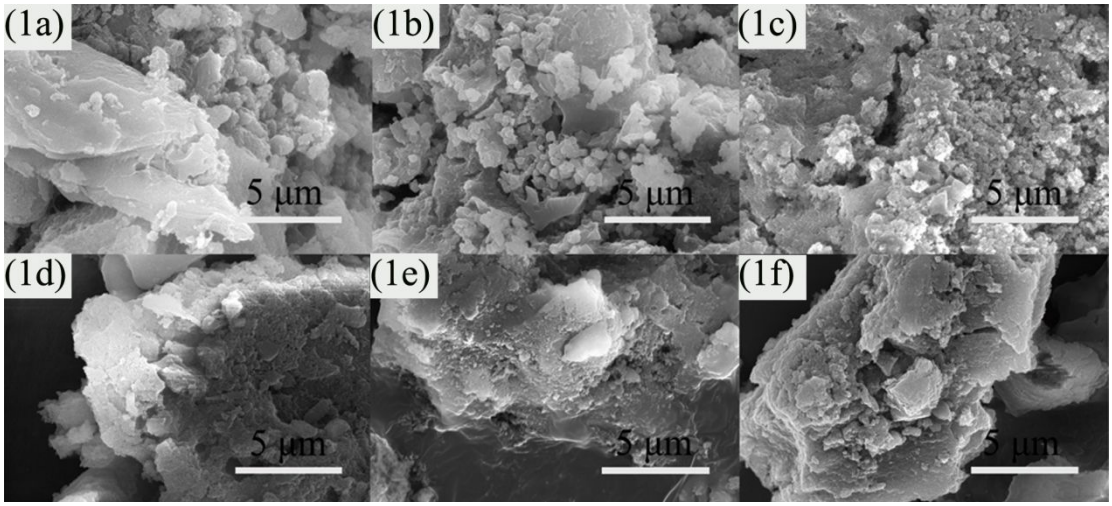

Figure S6. FE-SEM images of PPBPI-H (1a), PPBPI-Mn (1b), PPBPI-Fe (1c), PPBPI-H-CR (1d), PPBPI-Mn-CR (1e) and PPBPI-Fe-CR (1f). Scale bar: 5 μm.

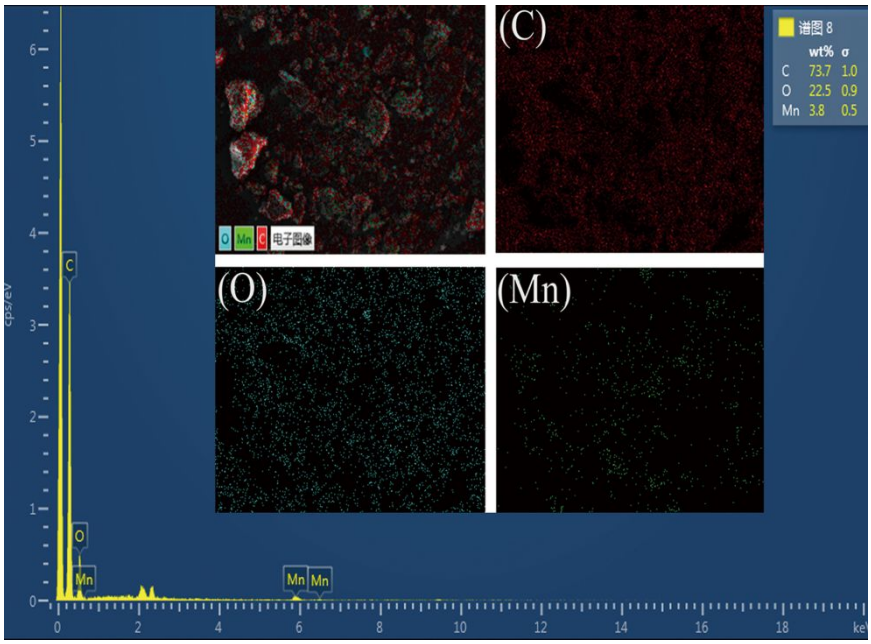

Figure S7. EDS mapping photographs of PPBPI-Mn-CR. The embedded images represented the distribution of carbon, oxygen and manganese.

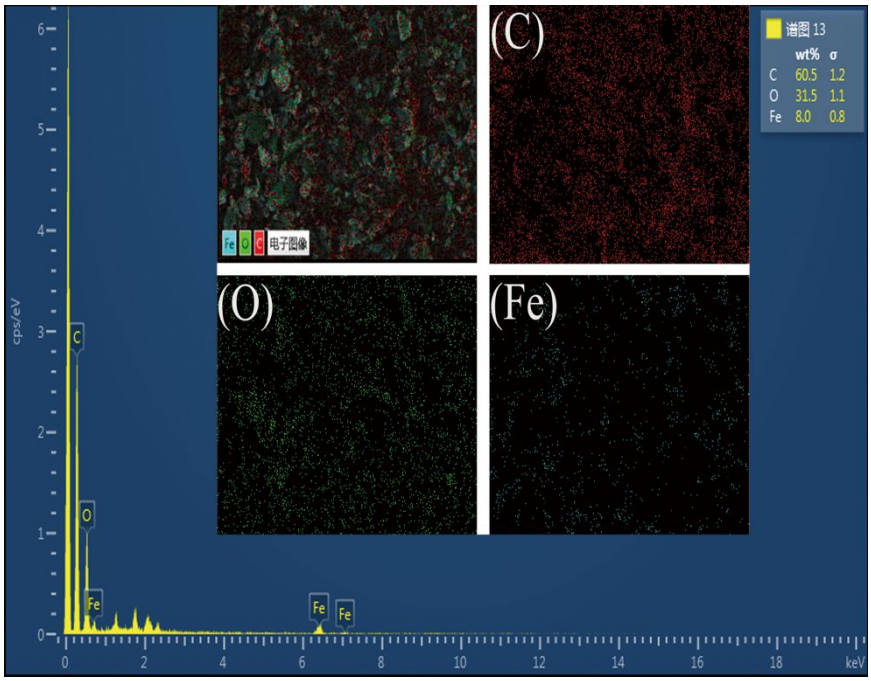

Figure S8. EDS mapping photographs of PPBPI-Fe-CR. The embedded images represented the distribution of carbon, oxygen and iron.

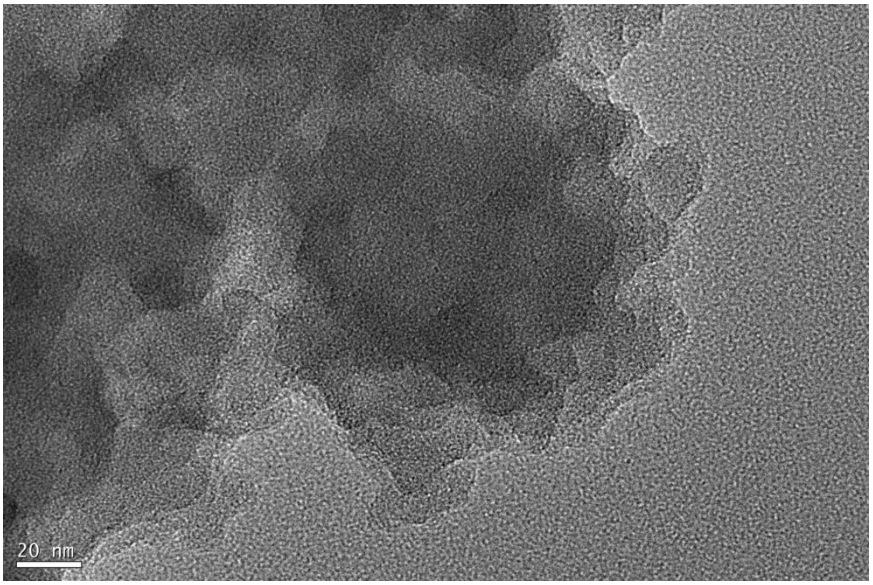

Figure S9. HR-TEM image of PPBPI-H-CR.

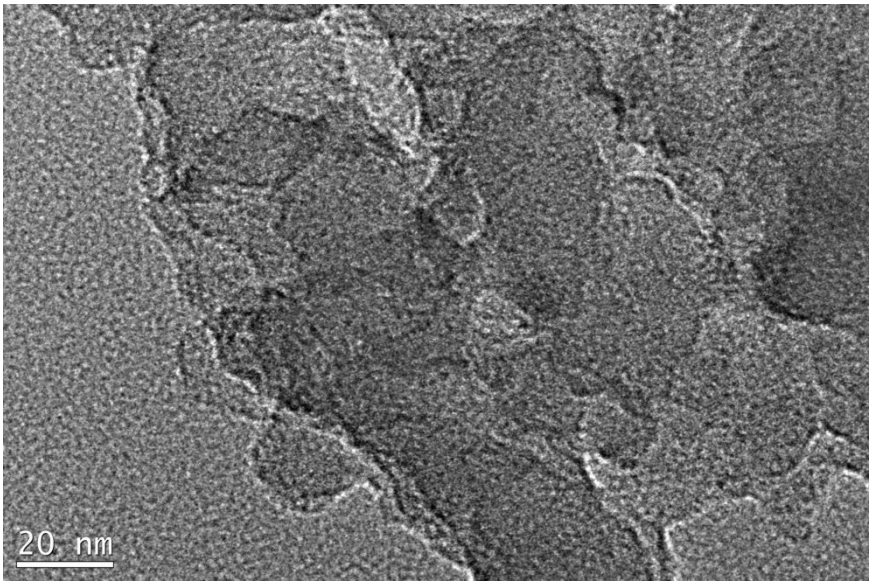

Figure S10. HR-TEM image of PPBPI-Mn-CR.

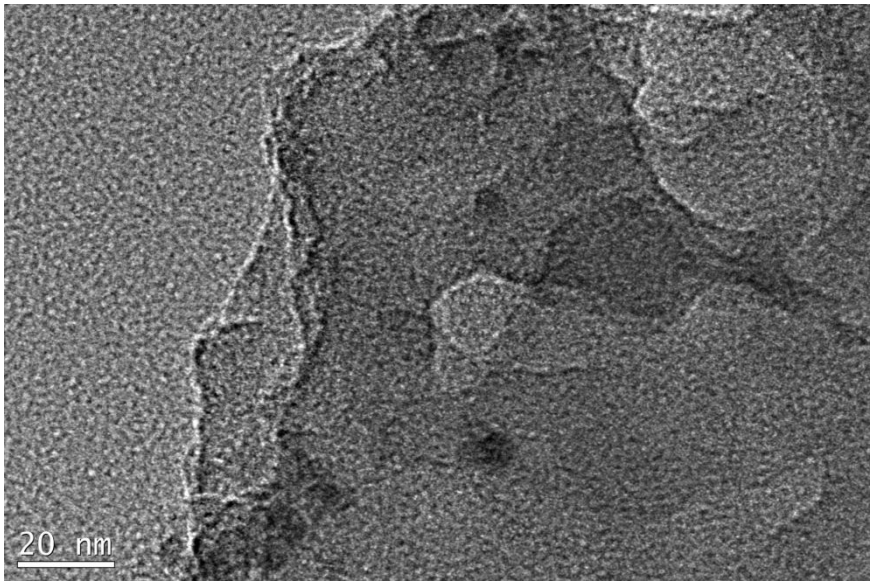

Figure S11. HR-TEM image of PPBPI-Fe-CR.

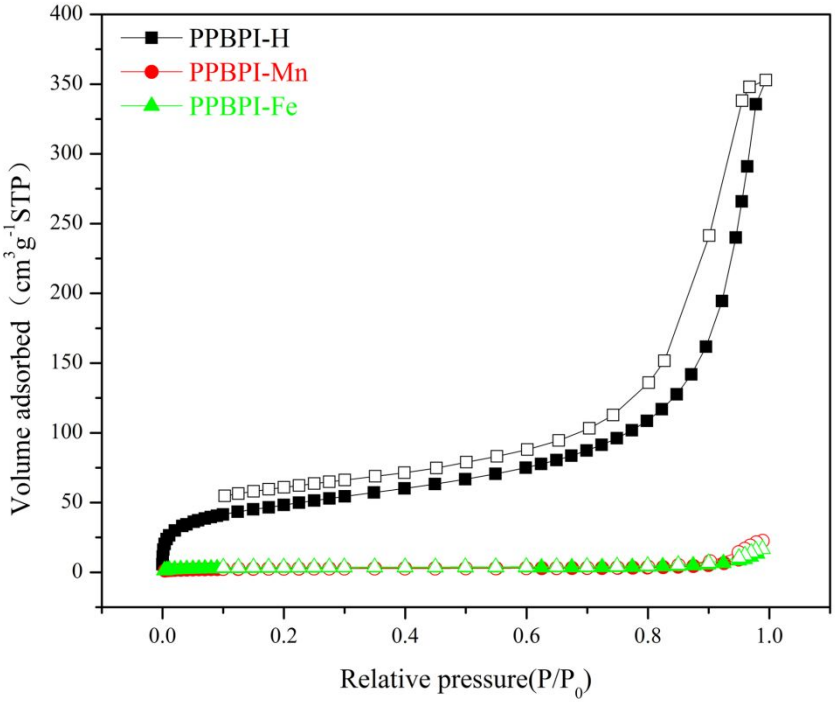

Figure S12. Adsorption (filled) and desorption (empty) isotherms of N_2 at 77 K for PPBPIs.

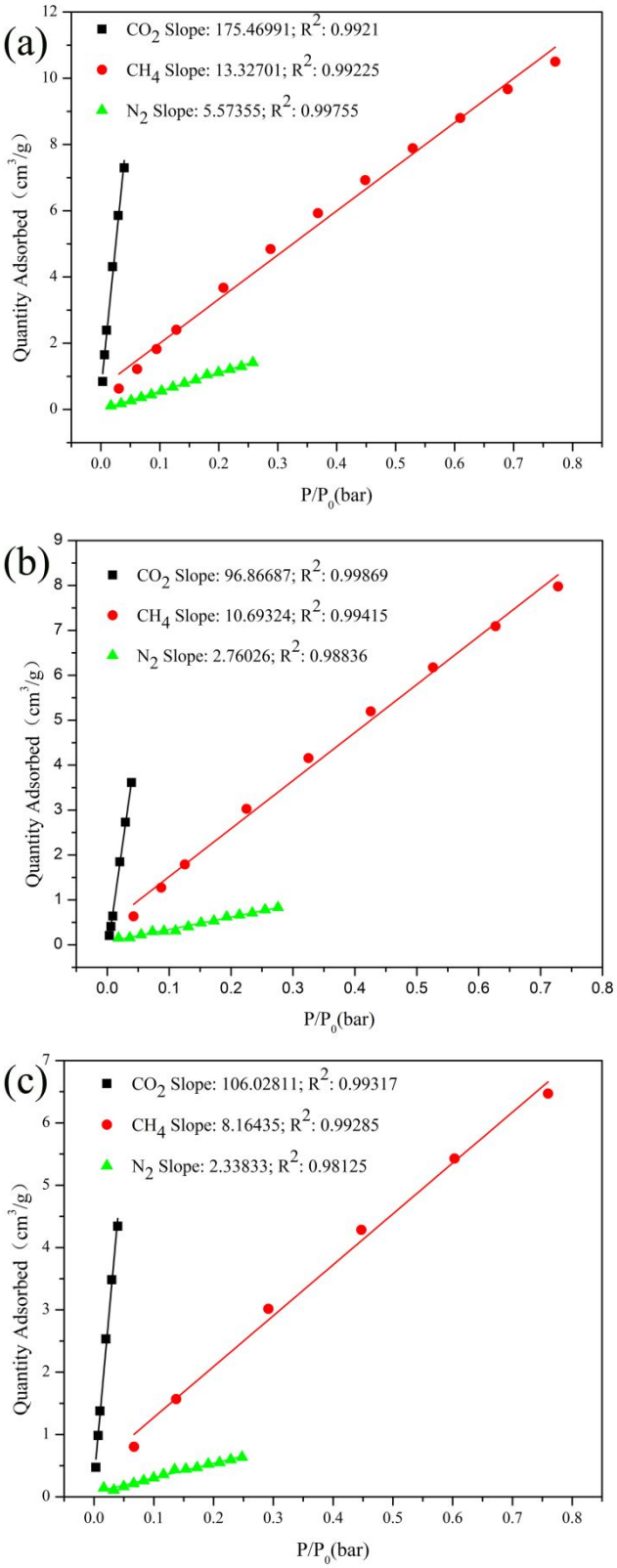

Figure S13. Adsorption selectivity of CO_2 over N_2 and CH_4 for PPBPI-H-CR (a), PPBPI-Mn-CR (b) and PPBPI-Fe-CR (c) from initial slope calculations, CO_2 (black), N_2 (green) and CH_4 (red) isotherms collected at 273 K.

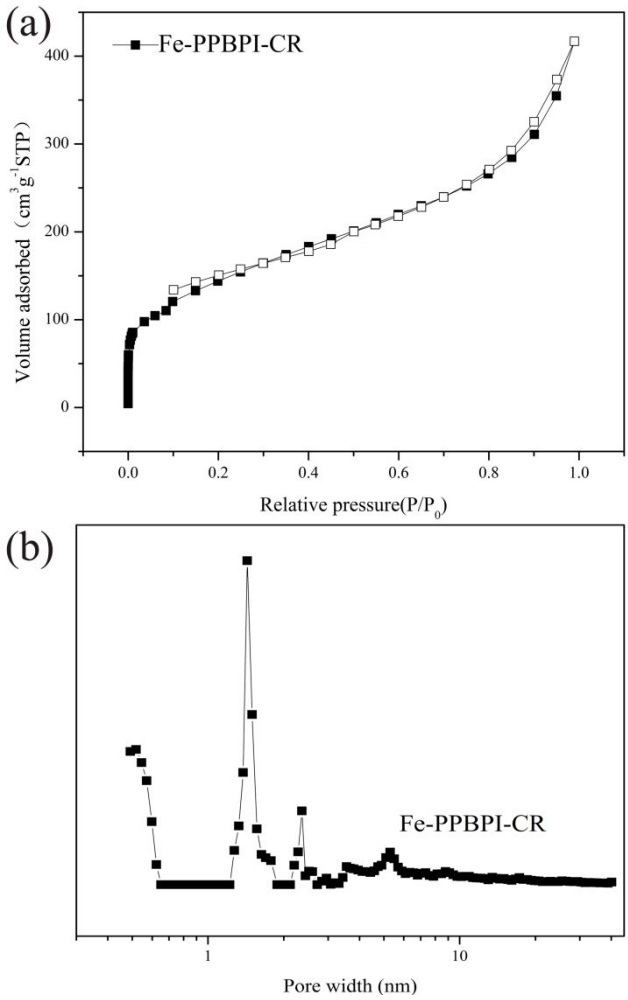

Figure S14. (a) Adsorption (filled) and desorption (empty) isotherms of N_2 at 77 K for Fe-PPBPI-CR, (b) pore size distribution of Fe-PPBPI-CR based on NLDFT method.

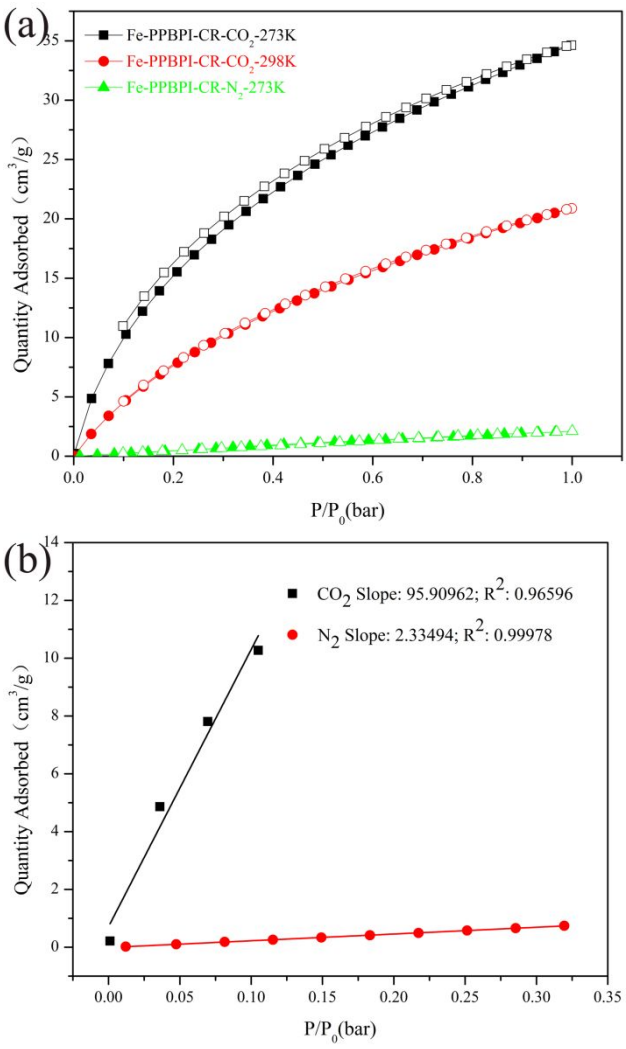

Figure S15. (a) CO_2 and N_2 adsorption and desorption isotherms for Fe-PPBPI-CR at 273 and 298 K, (b) adsorption selectivity of CO_2 over N_2 for Fe-PPBPI-CR.

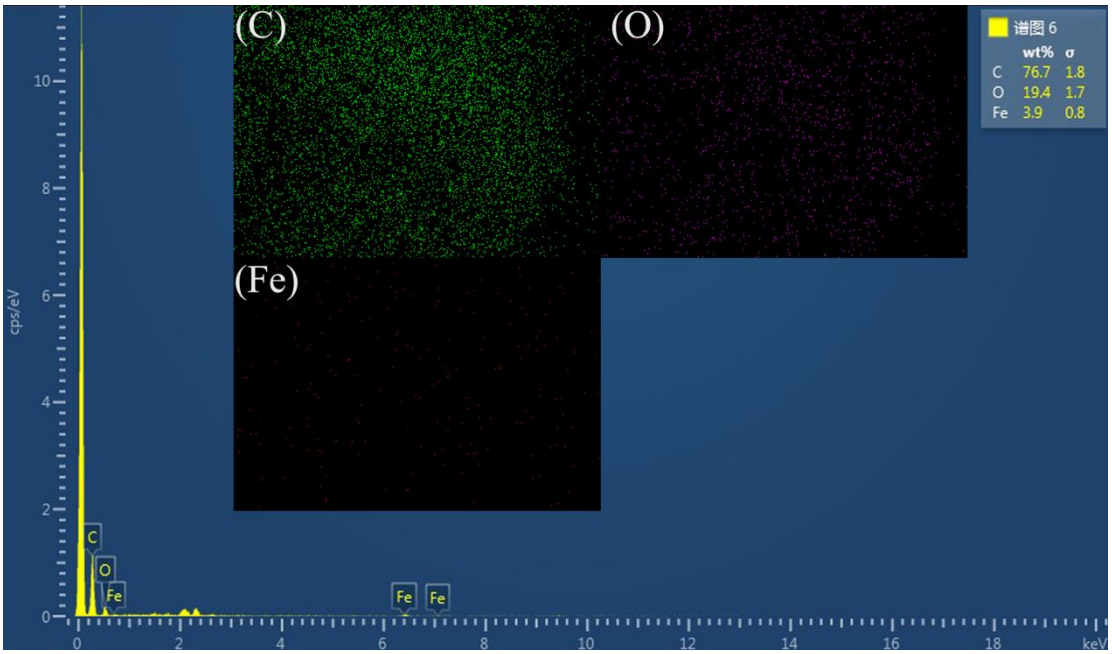

Figure S16. EDS mapping photographs of Fe-PPBPI-CR. The embedded images represented the distributions of carbon, oxygen and iron.

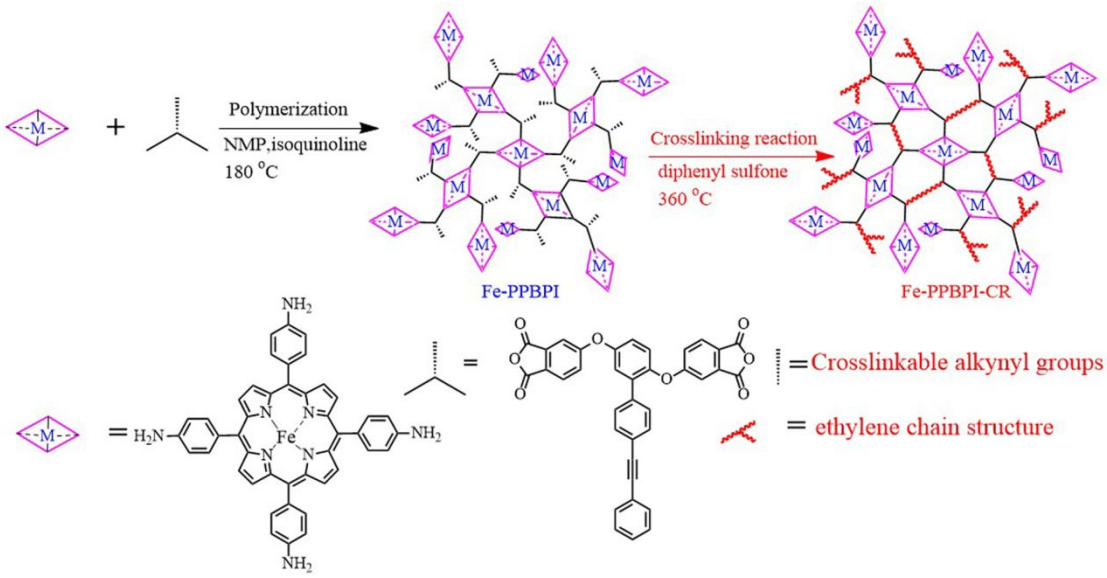

Scheme S1. Synthesis routes to crosslinked metalloporphyrin-based polyimide network (Fe-PPBPI-CR) from metalloporphyrin-based monomer.